Aerodynamic analysis of Ampyx's airborne wind energy system

IOP Conf. Series: Journal of Physics: Conf. Series **1037** (2018) 062008 doi:10.1088/1742-6596/1037/6/062008

Aerodynamic analysis of Ampyx's airborne wind energy system

K. Vimalakanthan[1], M. Caboni[1], J.G Schepers[1], E. Pechenik[2], P.Williams[2]

[1] Energy Research Centre of the Netherlands (ECN), 1755LE Petten, The Netherlands
[2] Ampyx Power, 2521AL Den Haag, The Netherlands

E-mail: kisorthman.vimalakanthan@tno.nl

Abstract.

Besides classical horizontal and vertical axis wind turbines, alternative ways to harvest wind energy are currently being explored. One promising concept is represented by airborne wind energy systems. Different airborne wind energy concepts have been ideated and investigated over the past few decades. The work reported here focuses on the concept being developed by Ampyx Power that basically generates power using a tethered airplane which drives a generator on the ground. The aim of the work reported here is to develop and compare design calculations for such a power plane. In this study a comparison was made between steady and unsteady RANS CFD calculations from SU2 and OpenFOAM. Subsequently, using the data from the CFD calculation two different power prediction models were developed and compared, one using 2D CFD data with the free vortex code AWSM and the other using the same data with a nonlinear lifting line approach to model the power plane in its figure eight flying trajectory. Overall, comparisons show that for all practical angles of attack, as well as a range of flap angles, that 2D CFD results agree extremely well between both solvers. The 3D CFD results show <20% differences on the computed total forces, despite achieving good agreement on the relative force contributions across the power plane. A very good agreement has also been established between the power prediction models.

1. Introduction

Ampyx Power's airborne concept generates electrical energy from wind energy by using a tethered rigid wing airplane with a ground based generator. On the ground, the tether is wound on a drum that drives the generator. The tether transfers the aerodynamic forces generated by the airplane to the ground, where it is converted into torque, and finally into electricity by the generator. The operational altitude varies with the wind speed, and is typically in the range between 250 and 500m. During the generation phase, the tether length increases, thus to complete the cycle, the tether is reeled-in as quickly as possible under very low tension. An example of the trajectory flown by the system is shown in Figure 1. The generation phase is characterized by cross-wind flight, in this case a lemniscate shape. The reel-in phase is characterized by flight towards the ground-based generator, in this case at a nearly constant altitude. For a more detailed description of the Ampyx Power's airborne system the reader is referred to [1] and [2].

Ampyx Power has developed a high-fidelity dynamic simulation model of its airborne wind energy system, which uses a 6-DOF rigid body model of the aircraft as the core element. The

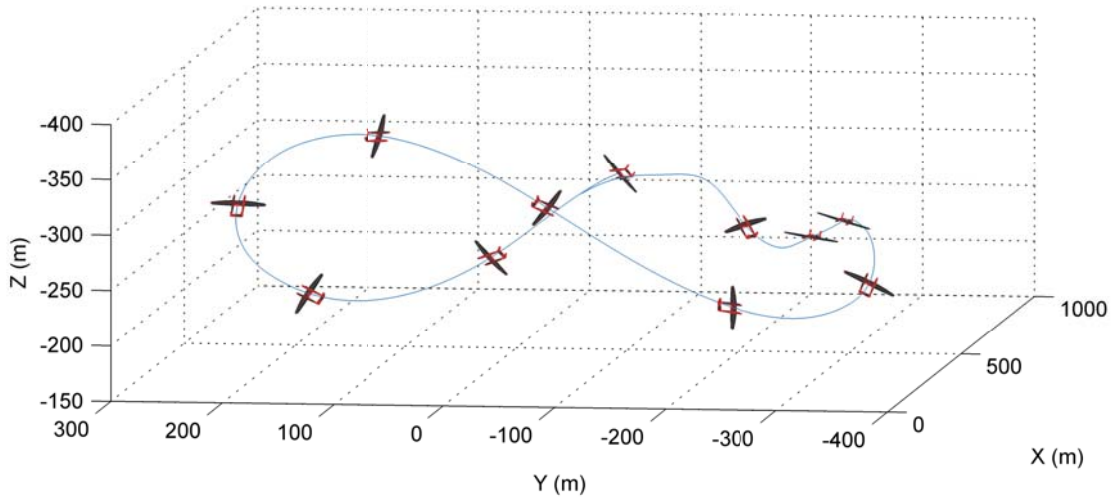

Figure 1. Example flight path over a complete power generation cycle.

rigid body model is coupled to a tether dynamic model [3], and a model of the generator. Models of the control surface actuation, sensors, and control system(s) are linked to the simulator to allow a complete end-to-end analysis of the system in different operating conditions. In this rigid wing airborne wind energy concept, the principle force producer is fundamentally an aircraft, and a nonlinear lifting line (NLL) code [4] using CFD data have been used to model the forces/moments acting upon it.

The continuous development of the Ampyx Power's airborne energy concept and, more generally, the development of airborne wind energy systems relies on verified tools and methodologies to be integrated in their design procedures. To this aim, the present paper's goal is at the one hand to verify the analysis model chain developed by Ampyx Power, and on the other hand to provide designers with an overview of verified tools and methodologies that can be confidently integrated in the design process of airborne wind energy systems. The verification to aerodynamic calculation procedure developed by Ampyx Power is here carried out using an alternative model chain incorporating different tools developed within ECN.

2. A verified model chain is fundamental to bring airborne wind energy to a mature level

The simulation chain devised by Ampyx Power to assess and optimize the aerodynamic performance of its powerplane includes two calculation steps. First of all, the powerplane wings' two-dimensional (2D) aerodynamic forces are calculated using a RANS CFD model. Then, the 2D forces are fed to a lifting line model to determine the overall forces of the powerplane and therefore to calculate its power production. Ampyx Power performs CFD simulations using OpenFOAM[5][6] and a code based on NLL approach. To verify this calculation chain, ECN developed an alternative chain using different tools, based on the RANS CFD SU2 code[7] and the lifting line/free vortex wake AWSM code [8]. This section compares these codes in two different subsections, the first focusing on the CFD models for the powerplane force computations and the second focusing on the lifting line approaches for overall power calculation.

This section is divided into two subsections, one dealing with the CFD models and the other one dealing with the lifting line models that makes the modeling chain. For each subsection the results and conclusion are presented within.

2.1. CFD methodology

The results from two open-source CFD solvers with different modeling approaches to simulate a powerplane are compared. Ampyx has used OpenFOAM's incompressible solver using segregated SIMPLE based algorithm with Rhi-Chow interpolation scheme (for pressure equation) to calculates the 2D and 3D aerodynamic performance of the plane, while ECN compares these results with the CFD solution from a density based solver SU2. Both solvers used the RANS equations for steady and unsteady state incompressible viscous flow. The k-omega SST turbulence model was used without wall function. Steady simulations with SU2 were performed using the Riemann based solver implementing the artificial compressibility method (ACM) and ROE scheme for convective flux discretization. The ACM is not valid for unsteady flow computations, thus all unsteady simulations with SU2 were performed with the pre-conditioned (ROE-Turkel) version of the compressible solver.

The 2D simulations modeled the multi element wing section at several operating angles of attack (AOA range between -2 to 20°) for various flap angles (FA ranging from -25 to 15°). All 2D simulations were performed for the Reynolds number of 3.05E6, that is calculated based on the maximum blade chord at the design wind speed of 15m/s. The 3D CFD simulations modeled the AP-3 power plane at three different operating scenarios: power production, side slip and landing.

2.1.1. Ampyx CFD model Ampyx's 2D OpenFOAM simulations were performed on hybrid grid consisting predominantly of triangle elements and quad elements near walls boundaries. Computational domain and boundary conditions for 2D problems are schematically illustrated on Figure 2. In order to keep refinement zone aligned with free stream flow, separate mesh was generated for every calculation case. 2D meshes contain approximately 180,000 cells including 25 quad layers near walls, where first prismatic layer height is 1e-05m to provide y+ values <2. These parameters were established based on an extensive grid refinement study and from validation with the NLR7301 airfoil under Mach=0.185, Re=2.51E6 at 13.1° AoA [9]. The gird independent solution achieved +2.8 and -25% difference with measurement in lift and drag respectively.

Solution convergence was analysed for every calculation case based on normalised residuals of governing equations (RMS<1e-7) and integral characteristics curves behavior.

The 3D OpenFOAM simulations from Ampyx were conducted with a hybrid grid (Figure 3) consisting predominantly of tetrahedral elements, while the boundary layers resolved with prisms. Computational domain and boundary conditions for 3D problems are shown in Figure 3. As with 2D simulations, every 3D calculation was performed using separate grids consisting of approximately 24million cells for half plane model, and 48million for full plane model. 3D meshes contain 25 prismatic layers near walls where first prismatic layer height is 5e-05m to provide y+ value of $\approx$ 5. The 3D CFD validation was performed based on the 2nd AIAA CFD High Lift Prediction Workshop [10] using the DLR F11 configuration 4 under Mach=0.175, Re=1.35E6 at two AoA of 0 and 12°. The results from the validation showed that the established model over predicts the lift and drag by 13, 8% respectively in comparison with measurements.

2.1.2. ECN CFD model ECN's 2D simulations were performed with a hybrid mesh (unstructured quad dominant, Figure 4) with 30 wall normal quad elements extending to 90chord with approx 200,000 elements. Different meshes were generated for different FAs. Contrary to Ampyx's model, the AoA for ECN simulation is set by the incoming flow field.

Numerical convergence was assessed based on the RMS residual (continuity, momentum, KE) < 1e-8 and K-Omega < 1e-5 with variation in lift coefficient < 5e-4 for all steady SU2 simulations. For all unsteady SU2 simulations, a periodic nature in the force history was used to evaluate numerical convergence. Using of the pre-conditioned compressible solver for solving

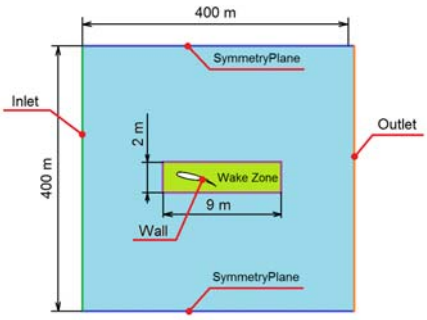

Figure 2. Computational domain used for 2D OpenFOAM simulations, Y+<2

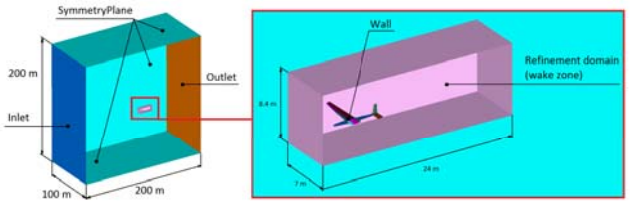

Figure 3. Computational domain used for 3D OpenFOAM simulations, Y+≈ 5

the unsteady incompressible flow severely restricted the flow residuals and it was only possible to attain RMS residuals on continuity < 1e-5, momentum and ke < 1e-3 and k-omega < 1e-0.5 for all SU2 unsteady simulations.

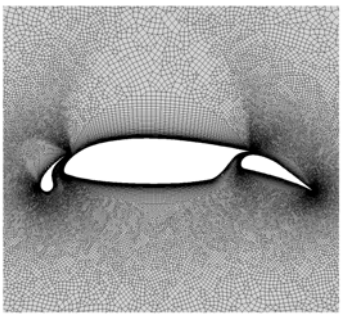

Figure 4. Close-up of the 2D unstructured quad dominant grid used for SU2 simulations, Y+≈ 1

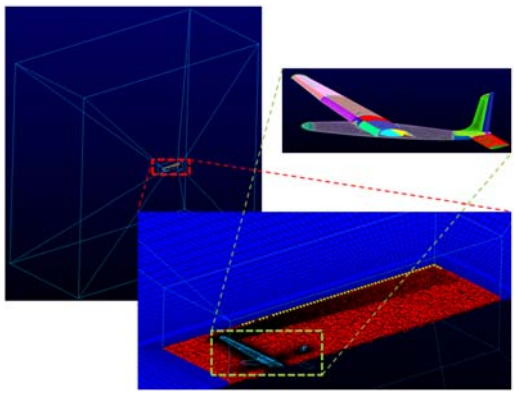

Figure 5. Hybrid grid used for 3D SU2 simulations, blue: hexahedra, red: tetrahedra, Y+≈ 5

ECN's 3D SU2 simulations were performed with a hybrid grid containing hexahedra elements within the boundary layer and outer volume, the flow field in between these two regions were resolved with tetrahedra elements (Figure 5). The transition region between the hexahedra and tetrahedra elements were modeled with pyramids. A conical refinement region to resolve the tip vortices was also incorporated. Consistent with Ampyx , a cuboid domain (Figure 3) with an extent of 30 plane lengths and a constant y+ value of 5 was consider for all plane surfaces based on the results from surface grid independence study. In this study the quadrilateral surface grid were increased by two folds, and additionally SU2 simulation were also performed with grid interdependent verified Ampex's grid, which showed negligible differences between them (<4% in lift and drag forces).

Three operating conditions were selected for the 3D comparison: power production, landing and side-slip, which are denoted as case 3, 28 and 50 respectively. The power production and

landing scenarios were simulated using only half of the power plane, with 18million element, while the full power plane geometry was simulated with 35million grid elements for side slip.

2.2. CFD results and comparison

In this section, the lift and drag coefficients calculated with ECN's SU2 and Ampyx's OpenFOAM CFD models are compared for two extreme FAs (-25 and 15°), as similar or better agreements were established in between. In general, the comparison indicates extremely good agreements between the calculated 2D performances from the two codes i.e. 2D CFD results are established independent of the CFD methods.

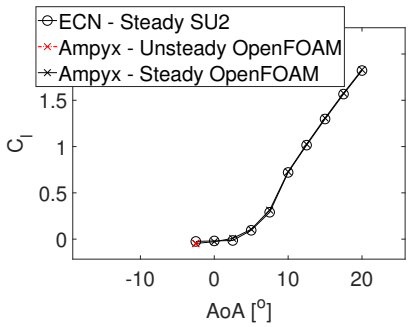

Figure 6. Lift polar for FA=-25°

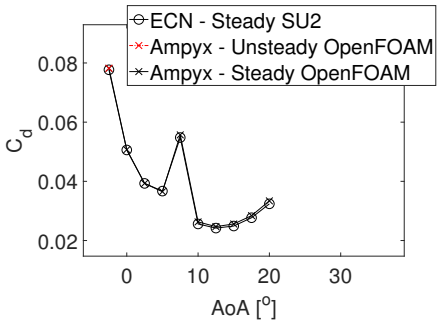

Figure 7. Drag polar for FA=-25°

The results for the large negative flap angle: -25° (Figure 6) clearly indicate that both solvers are in very good agreement with each other. At this FA, the calculated steady Cl values from SU2 and OpenFOAM differ by +/-0.025, while a maximum difference of 3% is calculated between the steady drag calculations. It is also noticeable that the trends in lift, drag and the spike at 7.5° AoA agree well between the two solvers. At this AoA, both solvers calculates a separation bubble that develops (and diminishes with larger AoA) at the nose of the main element, which results in a trailing edge separation of the main element.

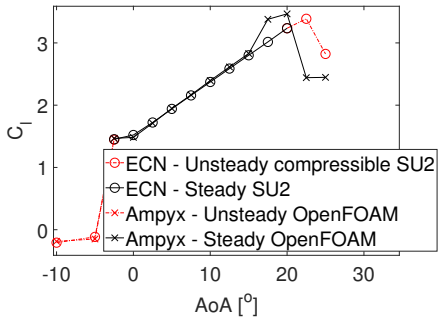

Figure 8. Lift polar for FA=15°

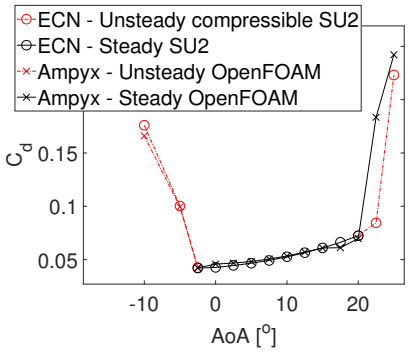

Figure 9. Drag polar for FA=15°

The comparison at FA = 15° shows that OpenFOAM's steady computation predicted a lower stall angle at 20°, while SU2 unsteady simulations predicted a constant stall AoA of 22.5°. This was seen for all FA between -5° to 15°. It is also at this non-linear region, larger differences are seen between SU2 and OpenFOAM. Within the operational region (AoA <15°), a good agreement is established between SU2 and OpenFOAM (dCl= 1%, AoA=15°) despite the large

FA. Throughout the investigated cases a similar agreements were also established on the moment coefficient comparisons. This suggests that not only the integrated forces are agreed well but also the computed pressure distributions are also consistent between the solvers.

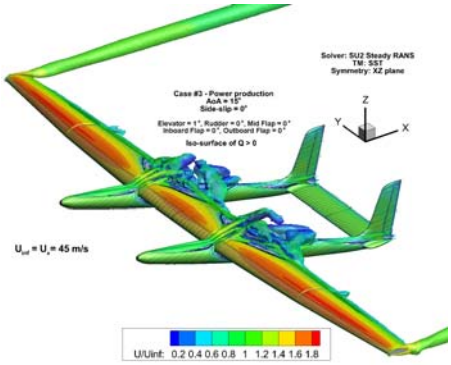

Figure 10. Flow separation structures (iso surfaces of Q>0) at power production (Case 3)

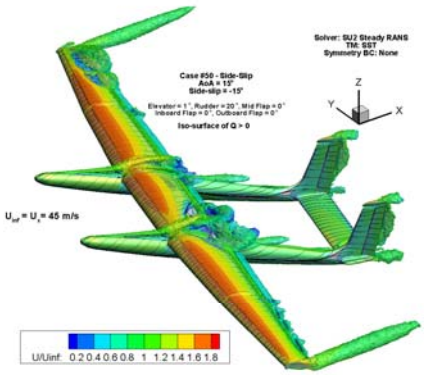

Figure 11. Flow separation structures (iso surfaces of Q>0) at side-slip operation (Case 50)

Based on the 3D CFD results (Figure 10 and 11), the force contribution from different part of the plane showed good agreement between the solvers (Figure 12). It was also evident that not only the scale but the corresponding trends agree well between the solvers i.e. both solvers identify the outboard wings as the largest lift contributor.

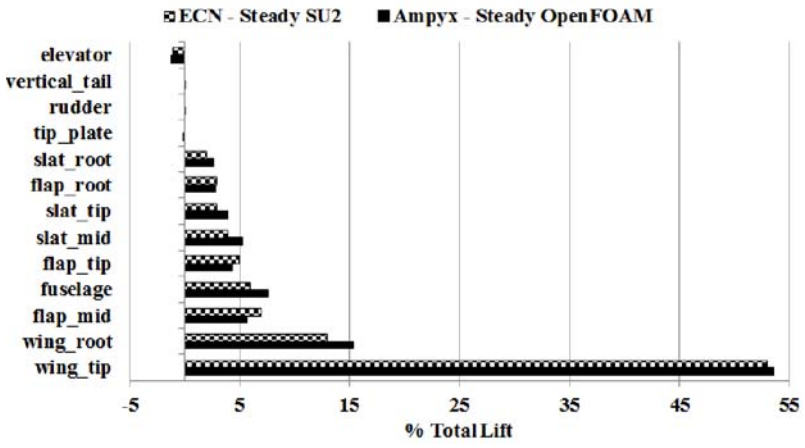

Figure 12. Lift contributions from different parts of the powerplane at power production phase

Overall comparison of the 3D results from steady OpenFOAM and SU2 shows a consistent 20% discrepancy between the computed lift and 11% on the drag forces (Table 1). OpenFOAM calculates higher lift characteristics than SU2, while larger drag forces are calculated with SU2, except at the landing scenario, where the unsteady OpenFOAM calculates 25% more drag forces than SU2. The results from OpenFOAM show an optimistic aerodynamic efficiency (Cl/Cd) of about 11.6 at the power production condition, while SU2 suggest a lower value of 8.33.

Table 1. Total aerodynamic force comparisons between OpenFOAM and SU2

Case	$Lift$ [kN]		$Drag$ [kN]	
	Ampyx (OpenFOAM)	ECN (SU2)	Ampyx (OpenFOAM)	ECN (SU2)
3	31.810	25.481 (-20%)	2.7512	3.0875 (+11%)
28	3.904 (Unsteady)	3.700 (-5%)	1.1255 (Unsteady)	0.8564 (-24%)
50	29.255	24.165 (-17%)	3.0710	3.4026 (+11%)

2.3. Lifting line methodology

Two different aircraft models using the 2D CFD data to determine the overall performance of the powerplane are compared. In Ampyx's NLL model, the forces/moments are modeled combining static and dynamic effects. Static contributions are determined by interpolating the force and moment coefficients as a function of flight condition (angle of attack, sideslip angle) and control surface position(s). Dynamic contributions are determined by incorporating stability derivative corrections to the static coefficients based on the aircraft angular rates, and rate of change of angle of attack and sidelip angle. The static force/moment coefficients are determined offline by sweeping the flight conditions and control surfaces using a nonlinear lifting line code [4]. The dynamic force/moment coefficients are determined using a vortex-lattice approach. ECN, with the same inputs as NLL model, compares its solution from lifting line/free vortex wake AWSM code [8].

2.3.1. Ampyx's NLL model The simulation environment used within Ampyx Power is designed for control law development and verification, as well as validation of system concepts. The same simulation models are also used for performing Hardware in the Loop verification of embedded software. To achieve these purposes, the simulation is performed using MATLAB/Simulink with highly efficient force models for all contributing elements in the system. Due to the nonlinear behavior of the wing forces and moments over the flight envelope, full aerodynamic lookup tables are created by sweeping a large combination of angle of attack and control surface deflections on the wing. This results in high dimension lookup tables that are interpolated during simulation. It is not feasible to generate these high dimensional lookup tables using 3D CFD.

The aerodynamic lookup tables are constructed via nonlinear lifting line based on the 2D CFD profile data generated by OpenFOAM. This approach was selected based on the combination of speed of convergence (fractions of a second) and the generally good accuracy of the method compared with 3D CFD. An example of the lift/drag polar at zero flaps is shown in 13. Note that NLL does not include fuselage or vertical tail drag and therefore slightly underpredicts the parasitic drag of the complete aircraft. Simulations are also performed using coarser lookup tables generated by 3D CFD for overall validation purposes.

2.3.2. ECN's free vortex wake model Aero-Module is an ECN software featuring current state-of-the-art wind turbine aerodynamic models [8]. The two aerodynamic methods included in Aero-Module are respectively a method based on the classical blade element momentum (BEM) theory [11], and a method based on the free vortex wake model coupled to the lifting line model [12], named Aerodynamic Wind turbine Simulation Module (AWSM). In this work, AWSM was used to calculate the aerodynamic forces generated by the powerplane during its flight path. The calculated aerodynamic forces were then used to estimate the airborne system's power production at different wind speeds.

The AWSM code require as user-defined kinematics (i.e., position and velocity) of the blades or wings, the sectional aerodynamic coefficients (lift, drag and moment polars) and the wind field.

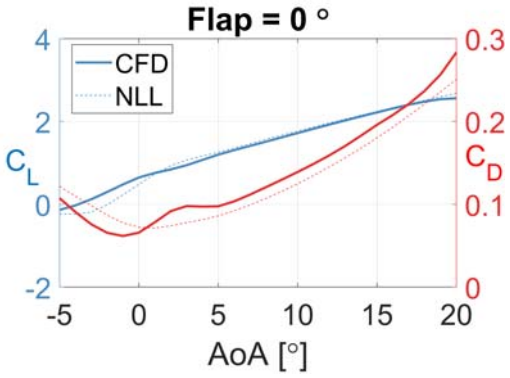

Figure 13. Example comparison of lift/drag polar between 3D CFD and NLL.

The airplane geometry has been modeled through 10 sections. Each of these sections carries a vortex ring from which the wake vortices are shed at each timestep. To better capture the effect of wing-tip vortices, the wing has been discretized through a full cosine distribution in the spanwise direction. The kinematics of each geometry element has been defined with its position, linear and angular velocity and orientation. In addition to the powerplane kinematics, the calculations also accounts for the flap settings along the flight path. The AWSM geometry model does not take into account the actual flap deformations, instead, the aerodynamic effect of the flap is incorporated via a 2D CFD polar data at the corresponding flap setting.

Figures 14 and 15 illustrates the airplane wake generated by AWSM, at a particular moment of its flight path, at the wind speed of 10 m/s. The contour in Figures 14 and 15 represent the strength of the wake's free vortices. The vortices' strength is related to the lift being generated by the profile at the moment in which the vortices were released from the wing. Once the vortices has been released from the wing, its strength remains constant. Warm colors therefore indicate that the wake points have been generated when the airplane's wings were producing hight lift, and vice versa.

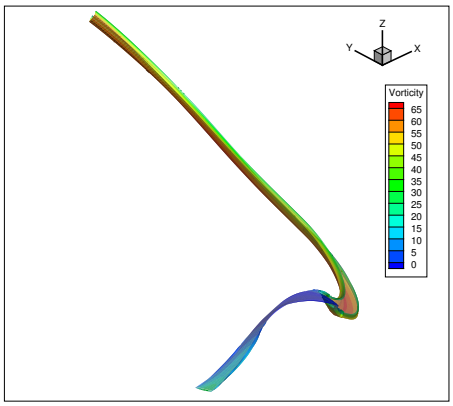

Figure 14. Airplane wake as calculated by AWSM. Contour represents vorticity from 0(blue)-65(red) m^2/s

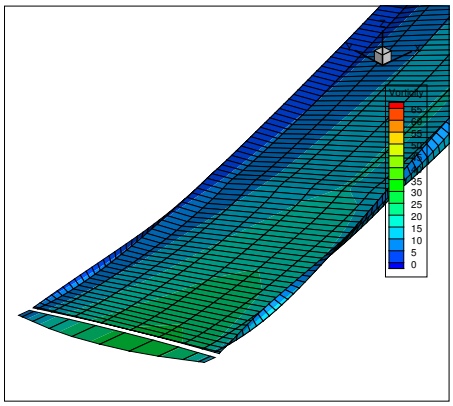

Figure 15. Detail of the wake in the airplane proximity. Contour represents vorticity from 0(blue)-65(red) m^2/s

2.4. Lifting line results and comparison

This section presents the comparison of power computation between Ampyx's NLL model and the simulations performed with ECN's AWSM code.

The calculation of power is based on the evaluation of the airplane's lift and drag determined by the lifting line models. At each time step the power generated by the airplane P is calculated as the product of the tether tension T and the tether velocity v_t, as $P = Tv_t$. The tether velocity is defined as the projection of the airplane velocity in the tether direction. The tether tension is equal to the sum of the lift, drag, inertial, and gravity forces projected in the tether direction.

Figures 16, 17 and 18 show the power generated by the aircraft as a function of time at wind speeds of 10 m/s, 15 m/s and 25 m/s. These figures indicate when the airplane is generating power in reel-out mode (positive power), and when it is actually absorbing power in reel-in mode (negative power). Figures 16, 17 and 18 show a general good agreement between Ampyx and ECN calculations in both trend and absolute values.

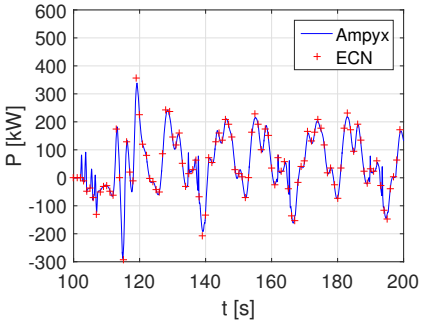

Figure 16. Power plane power as a function of time at a wind speed of 10 m/s.

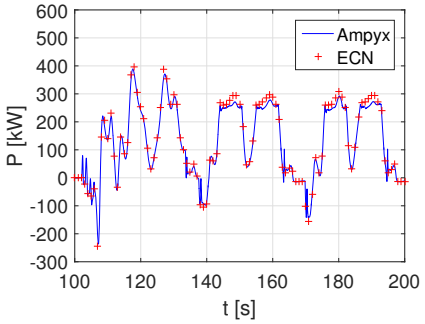

Figure 17. Power plane power as a function of time at a wind speed of 15 m/s.

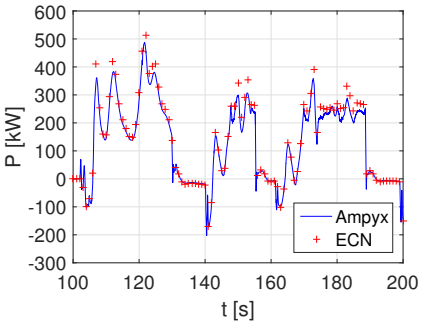

Figure 18. Power plane power as a function of time at a wind speed of 25 m/s.

Finally, the average power over one cycle is compared in Table 2. It is seen that ECN calculations predict larger power with respect to Ampyx's calculations at all wind speeds. The differences are $\leq 5\%$ for wind speed of 10 and 15 m/s. The largest differences is seen at 25 m/s, when the relative difference is 14%. As shown in the power comparison above, the differences between ECN and Ampyx predictions grow as the wind speed increases. The reason behind these differences is tied to the different approach followed to model the effect of the flap. At higher wind speeds the flap is more frequently used to control the airplane power.

Table 2. Average airplane power over one cycle.

u [m/s]	$\bar{P}$ [kW]	
	Ampyx	ECN
10	63	65 (+3%)
15	130	137 (+5%)
25	118	135 (+14%)

3. Conclusion and future challenges

In this study a comparison was made between 2D steady and unsteady calculations from SU2 and OpenFOAM. Calculations are performed for different flap angles and different angles of attack. Moreover, 3D steady SU2 results are compared to those from Ampyx obtained with OpenFOAM for three different scenarios. Overall comparison show that for all tested angles of attack (AoA=-10 to 22.5°) at different flap angles (FA=-25 to 15°) 2D results agree extremely well between both solvers. However the 3D results comparison show <20% differences on the computed absolute forces, despite achieving good agreement on the relative force contributions across all parts of the power plane. Comparing the free vortex model against the non-linear lifting line power prediction model has shown very good agreement between Ampyx Power and ECN models.

The future challenges exists at validating the presented modeling chain. Extensive flight test validation campaigns are planned and will be commenced when the airframe and subsystems are completed. Flight validation of the bare airframe characteristics will be performed for both quasi-static and dynamic environments. Quasi-static (trim) conditions will be used to validate the lift/drag polars, whereas dynamic tests will be used to validate the influence of maneuvering on the aerodynamic model. An extension of the presented model to evaluate multiple powerplanes with their wake interactions is also planned for the future, which will provide the essential tools to evaluate energy production of airborne wind farm of this type.

4. References

[1] Sieberling S and Ruijterkamp R 2011 The PowerPlane an Airborne Wind Energy System Conceptual Operations *11th AIAA Aviation Technology, Integration, and Operations (ATIO) Conference* (Virginia Beach, VA, USA)
[2] Ruijterkamp R and Sieberling S 2014 Description and Preliminary Test Results of a Six Degrees of Freedom RigidWing Pumping System *Airborne Wind Energy* ed Ahrens U, Diehl M and Schmehl R (Springer) chap 26, pp 443–458
[3] Williams P *Journal of Guidance, Control, and Dynamics* **40** 1779
[4] JD Anderson S Corda D V W *Journal of Aircraft* **17** 898
[5] Weller H G, Tabor G, Jasak H and Fureby C 1998 *Computers in physics* **12** 620–631
[6] Jasak H, Jemcov A and Tukovic Z 2007 Openfoam: A c++ library for complex physics simulations *International workshop on coupled methods in numerical dynamics* vol 1000 (IUC Dubrovnik, Croatia) pp 1–20
[7] Palacios F, Colonno M, Aranake A, Campos A, Copeland S, Economon T, Lonkar A, Lukaczyk T, Taylor T and Alonso J 2013 *AIAA Paper* **287**
[8] Boorsma K, Grasso F and Holierhoek J 2011 Enhanced approach for simulation of rotor aerodynamic loads *Proceedings of EWEA Offshore 2011* (Amsterdam, The Netherlands)
[9] Vandenberg B and Gooden J 1994 *In AGARD, A Selection of Experimental Test Cases for the Validation of CFD Codes,* **2**
[10] Rumsey C L and Slotnick J P 2014 *Journal of Aircraft* **52** 1006–1025
[11] Manwell J, McGowan J and Rogers A 2002 *Wind Energy Explained. Theory, Design and Application* (John Wiley and Sons Ltd.)
[12] Kats J and Plotkin A 2010 *Low-Speed Aerodynamics. Second edition.* (Cambridge University Press)